TISSUE ENGINEERING: Part A
Volume 19, Numbers 13 and 14, 2013

DOI: 10.1089/ten.tea.2012.0585

Nanoporosity Significantly Enhances the Biological Performance of Engineered Glass Tissue Scaffolds

Shaojie Wang, PhD,[1] Tia J. Kowal, BS,[3] Mona K. Marei, PhD,[2]
Matthias M. Falk, PhD,[3] and Himanshu Jain, EngScD[1]

Nanoporosity is known to impact the performance of implants and scaffolds such as bioactive glass (BG) scaffolds, either by providing a higher concentration of bioactive chemical species from enhanced surface area, or due to inherent nanoscale topology, or both. To delineate the role of these two characteristics, BG scaffolds have been fabricated with nearly identical surface area (81 and $83 \pm 2\,m^2/g$) but significantly different pore size (av. 3.7 and 17.7 nm) by varying both the sintering temperature and the ammonia concentration during the solvent exchange phase of the sol-gel fabrication process. *In vitro* tests performed with MC3T3-E1 preosteoblast cells on such scaffolds show that initial cell attachment is increased on samples with the smaller nanopore size, providing the first direct evidence of the influence of nanopore topography on cell response to a bioactive structure. Furthermore, *in vivo* animal tests in New Zealand rabbits (subcutaneous implantation) indicate that nanopores promote colonization and cell penetration into these scaffolds, further demonstrating the favorable effects of nanopores in tissue-engineering-relevant BG scaffolds.

Introduction

Dysfunctional tissues are repaired routinely by using implants made from biomaterials.[1] Notwithstanding, a superior approach has been gaining attention in recent years, which is based on tissue engineering: rather than providing an implant as a replacement for the diseased tissue, a scaffold is implanted. An ideal bioscaffold would not only provide a three dimensional (3D) structure to facilitate the regeneration of natural tissue, but also degrade gradually and, eventually be replaced entirely by the natural tissue.[2] For the regeneration of bone, bioactive glass (BG) scaffolds are particularly attractive. They not only exhibit high biocompatibility and ease of fabrication in complex shapes at low costs, but also stimulate tissue growth at the gene level.[3]

A few criteria have been proposed for an ideal bioscaffold that include biocompatibility, biodegradation, and high porosity with interconnected pores hundreds of microns in diameter to allow tissue ingrowth and nutrient delivery to the newly formed tissue.[4–9] Various techniques have been developed to generate porous bioactive ceramic/BG scaffolds, including polymer sponge replication,[10–13] 3D printing,[14] dry pressing,[15–17] freeze casting,[18] and glass fiber sintering.[19] In most of these synthesis methods, melt-quench-derived micrometer-sized BG particles are used as the starting material. Therefore, only micrometer-sized large pores (macropores) are produced, which usually lead to an insufficient degradation rate. In this regard, nanopores can be added to tailor the degradation process of the scaffold, since they dramatically increase the surface area ($\geq$10-fold), leading to a significantly higher degradation rate.[20] An ideal scaffold for hard tissue regeneration will then have both nano- and macropore (termed tailored amorphous multi-porous [TAMP]) structure that is simultaneously optimized for tissue ingrowth and degradation. Recently, nano–macro porosity has been introduced by specialized heat treatment for multi-scale phase separation followed by leaching.[21] In parallel, since nanopores are inherent to the sol-gel method of glass fabrication, sol-gel-derived materials have been used for TAMP bioscaffold fabrication, for example, using the sol foaming method,[22] the sol-gel process with spinodal decomposition,[23,24] and sol-gel method combined with sponge replication.[25]

Intensive research over the past years has shown that nanostructured materials, characterized by dimensions of less than 100 nanometers, are indeed promising for a wide range of advanced technologies, including medical applications.[26] As such, nanostructured materials are developed or applied as carriers for targeted drug and gene delivery, as tracers for bioimaging, tools for nanoscale surgery, components of nanoelectronic biosensors, and especially as cell carriers for tissue engineering.[27] Furthermore, incorporation of nanostructure, such as nanocarbon/-polymer fibers or

[1]Department of Materials Science and Engineering, Lehigh University, Bethlehem, Pennsylvania.
[2]Tissue Engineering Laboratory, Faculty of Dentistry, Alexandria University, Alexandria, Egypt.
[3]Department of Biological Sciences, Lehigh University, Bethlehem, Pennsylvania.

nanopores, of various material systems is shown to have beneficial effects on cell functions.[28–36] However, the precise role of nanopores in BG scaffolds on surrounding tissue and cells has not been explored fully, although indications of improved cell response on nanoporous versus nonporous BG have been reported.[34] In most of these studies, the significance of nanostructure to cell function was established from the observations comparing cell response to two types of materials: conventional materials without nanostructure and materials with nanostructure. Unfortunately, multiple parameters have been varied in these investigations, making the role of nanoporosity ambiguous and questionable.

Several methods have been proposed to tailor the nanoporosity of glass prepared by the sol-gel method: (I) by changing the gelation time,[37] (II) by introducing a condensation inhibitor in the sol-gel process,[38] (III) by sintering the nanoporous BG material at different temperatures,[39] and (IV) by solvent exchange during the aging process in sol-gel-derived materials.[40] However, in all of these methods, the change of nanopore size is always associated with a concurrent variation of surface area. Therefore, the evaluation of material with different nanopore size tailored by these methods has included the combined influence of (a) surface area related effects, for example, chemistry of surrounding liquid medium and protein adsorption, and (b) the purely topographical effects of nanopores. In fact, despite numerous studies suggesting the impact of nanostructure on cell function in various materials,[28–33,36] there has been no direct evidence showing unambiguously whether the observed influence resulted from change in surface area or nanotopography. To decouple the role of these two fundamentally different attributes, it is imperative to fabricate bioscaffolds that feature comparable surface area but significantly different pore sizes. This can be a challenging task as generally the two factors vary concurrently during the fabrication process.

In this study, we have applied solvent exchange and sintering techniques to tailor the nanoporosity of TAMP scaffolds. Solvent exchange dramatically enlarged the nanopore size, whereas sintering reduced the pore size. Combining the two techniques resulted in the fabrication of samples featuring almost identical surface areas (81 and $83 \pm 2\,m^2/g$) but significantly different nanopore size (3.7 and 17.7 nm). The impact of surface area versus nanotopography on the performance of the TAMP scaffolds was tested by comparing *in vitro* cell and *in vivo* tissue responses. We found that initial cell attachment was increased on samples with smaller nanopore size, and that nanopores promoted colonization and cell penetration into the scaffolds. These results demonstrate for the first time the beneficial effect of nanopore topography in tissue-engineering-relevant BG scaffolds.

Materials and Methods

Fabrication of TAMP scaffolds

The BG scaffold of 70% SiO_2–30% CaO composition is fabricated by combining the sol-gel process with spinodal decomposition as described previously.[41] To eliminate variation in sample characteristics from initial processing conditions, we fabricated a large batch of 48 samples, which were then subjected to different final treatment (solvent exchange and sintering temperature) that controlled only the pore size. All data shown here were obtained on samples from this batch. Briefly, 9 mL tetramethyl-orthosilicate (TMOS) and 6.18 g $Ca(NO_3)_2 \bullet 4H_2O$ were added into a solution, which was made by dissolving 1.4 g polyethylene oxide (PEO, molecular weight 100,000) into 20 mL 0.05N acetic acid. After vigorous stirring, 2.5 vol.% HF was added to catalyze gelation, followed by further stirring for ~20 s. Then, the sol was immediately cast into wells of tissue culture plates. Gelled samples were aged at 40°C for 1 day, and then soaked in distilled water or ammonia solution for 3 days for solvent exchange before they were dried and stabilized by sintering at 700°C. We varied the concentration of ammonia solution (0.01N, 0.1N, 1N, 3N) to tune the nanopore size. For comparison, one batch of samples was aged for 4 days without solvent exchange.

We varied the sintering temperature to partially close the nanopores and tailor the surface area of the BG scaffolds. In this case, the solvent exchange step was skipped and the aged samples were directly dried, stabilized at 600°C, and then furnace-cooled. These BG scaffolds were then reheated to a specific sintering temperature at the rate of 10°C/min, held for 2 h before cooling down to room temperature. The sintering temperature was selected as 700°C, 750°C, 800°C, 840°C, or 1000°C to examine its influence on nanoporosity.

Characterization of the nanoporosity of TAMP scaffolds

To characterize the nanopore network directly, samples were examined by transmission electron microscopy (TEM). A scaffold was finely ground using a mortar and pestle. The porous glass powder was mixed with anhydrous absolute ethyl alcohol, and ground for 5 min. A drop of the glass-powder/ethyl alcohol slurry was transferred onto a lacey carbon-coated 300-mesh copper grid (SPI# 3830C-FA), which was loaded into a TEM specimen chamber (JOEL 2000) after air-drying for 10–15 min, and then examined with an electron accelerating voltage of 200 kV.

Specific surface area and nanoporosity were determined by nitrogen adsorption (ASAP 2020; Micromeritics) BET[42] and BJH methods[43] using adsorption and desorption curves, respectively. For these experiments, weighed specimens were evacuated and heated at 150°C for at least 5 h to remove any trapped moisture and potential surface contaminants before analysis. When the porosity of nine samples from the same batch was measured, the average value varied within 2.6%, which indicates the experimental uncertainty in porosity results described in Figures 1A, 2A, 3A, and 5A.

In vitro *cell response of TAMP scaffolds*

MC3T3-E1 subclone 4 newborn mouse calvarial bone preosteoblast cells (ATCC, CRL-2593) were chosen as the model to study cell response to our samples. Cells were maintained under standard conditions as recommended by American Type Culture Collection (ATCC). The autoclave-sterilized glass scaffolds were seeded with cell suspension at a final density of 800 cells/mm^2, and placed into an incubator at 37°C, 5% CO_2, 95% air, and saturated humidity. The samples were washed with phosphate-buffered saline (PBS) to remove unattached, or only weakly attached cells at 12 and 48 h postseeding. Cells remaining on the sample were fixed with 3.7% formaldehyde, washed with PBS, permeabilized with 0.2% Triton X-100, and then washed again with

PBS. Next, cells were stained with 1:200 dilution of Alexa Fluor 488–labeled Phalloidin (Invitrogen/Molecular Probes) and 1:1000 dilution of DAPI (Invitrogen/Molecular Probes) solution (1 mg/mL stock in water) for the visualization of cytoskeletal F-actin and cell nuclei, respectively. Finally, three areas of each sample (three samples of each type) were examined by fluorescence microscopy (Nikon Eclipse TE2000U). For quantitative analyses, cell density was determined by manually counting the cells in each area. To obtain larger focus depths low magnification (4×, 10×, and 20×) long-distance air objectives were used.

In vivo *testing of TAMP bioscaffolds implanted into New Zealand rabbits*

For animal *in vivo* tests, specimens were sterilized by autoclaving for surgical implantation into white male New Zealand rabbits. Samples used for all analyses in this study were typically in disk shape with ~12 mm diameter and ~2 mm thickness. Guidelines for the care and use of laboratory animals were followed in all experiments.[44] General anesthesia was administered using Xylazine HCL 2% in a dose of 20 mg/kg body weight followed by Ketamine HCL in a dose of 100 mg/kg body weight intraperitoneally. Four subcutaneous pouches, separated by approximately 2 cm, were created on the dorsal surface of the animal. The TAMP scaffolds were implanted into the pouches that were made in size to just encompass the samples, and shallow enough to maintain the underlying fascia intact. The wounds were then sutured using 3.0 silk suture material.[45]

At 1 and 2 weeks postsurgery, full thickness specimens including the implants were excised, immediately placed in 10% formalin fixative, and stepwise dehydrated in graded concentrations of ethyl alcohol. Specimens were cleaned in xylene, followed by embedding in methyl methacrylate resin (Aldrich) for histological hard-section preparation. Then, they were treated with Stevenel's blue (stains connective tissue bluish-green) and Van Gieson's (stains hard tissue red) (Bio-Optica).[46] Sections were examined and imaged using an Olympus light microscope (Model CH40).

Results

In this study, all data were obtained on samples from the same batch, which was also used in biological testing. In general, at least three samples were used in parallel. Thus, any batch-to-batch variation in composition was eliminated, and results presented below are likely to represent the effect of pore characteristics only.

Tailoring nanopores by sintering

Two different methods were used to tailor the nanopores of BG scaffolds: sintering and solvent exchange. The direct effect of sintering temperature on the pore size distribution, median nanopore size, the surface area, and the nanopore volume (which is contained in pores ranging in size from 1.7 to 300 nm) of the BG scaffolds, as measured by nitrogen adsorption porosimetry, is shown in Figure 1A. Both surface area and nanopore volume dramatically decreased, whereas the median pore size decreased only slightly as the sintering temperature increased. These observations indicate that nanoporosity can be eliminated readily by sintering at relatively high temperatures.

During sintering, a porous material would reduce excess energy associated with surfaces by following two different pathways: coarsening and/or densification with correspondingly different but competing atomic mechanisms.[47] If the atomic process leads primarily to densification, the pore volume would decrease dramatically (Fig. 1B, panel a). However, if coarsening dominates, the pore size would significantly enlarge while pore volume remains relatively unchanged (Fig. 1B, panel b). Thus, the results shown in Figure 1A suggest that the sintering process in our TAMP scaffolds is dominated by the densification mechanism. Furthermore, when the sintering temperature is increased, the magnitude of the change in surface area is larger than that in the nanopore volume. For instance, when the sintering temperature is increased from 700°C to 1000°C, the surface area is reduced by a factor of 1/32, whereas nanopore volume shrinks to 1/11. This difference is presumably because the driving

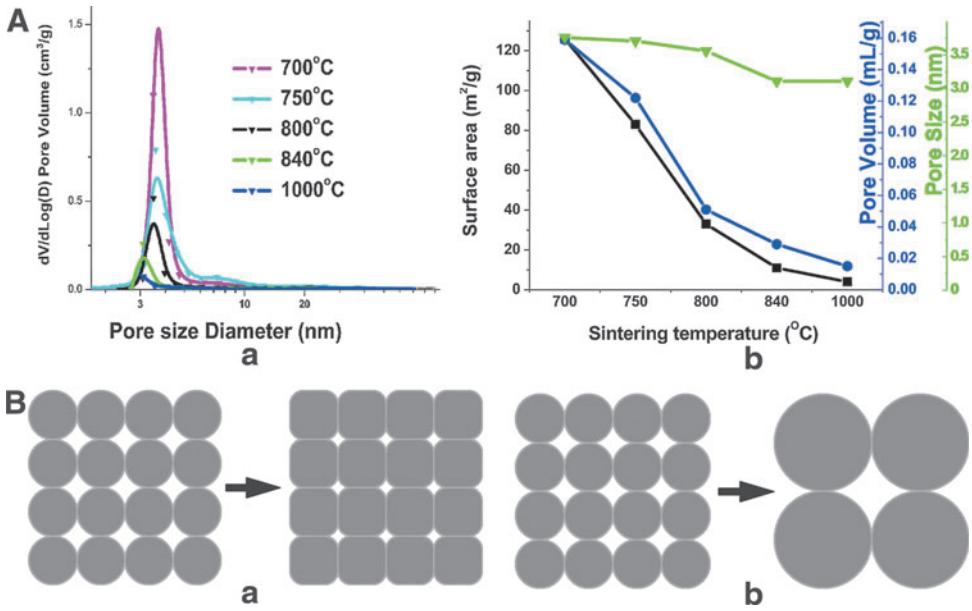

FIG. 1. **(A)** Effect of sintering temperature on pore size distribution **(**in **a)**, and surface area (black squares), nanopore volume (blue circles), and median nanopore size (green triangles) **(**in **b)** of TAMP scaffolds. At least three samples were analyzed in parallel in this analysis, and in the analyses presented in Figures 2A, 3A, and 5A. **(B)** Schematic representation depicting two possible paths that can lower surface energy: **(a)** densification and **(b)** coarsening. TAMP, tailored amorphous multi-porous. Color images available online at www.liebertpub.com/tea

force for densification is greater for smaller pores; hence, they would be eliminated preferentially. For a given pore volume, small pores provide a larger surface area than large pores. Therefore, the sintering process reduces the surface area much more than the pore volume.

Tailoring nanopores by solvent exchange

Besides sintering, we have exploited solvent exchange of ammonia with acetic acid present in the gel network to manipulate nanopore size. The nitrogen adsorption porosimetry results for samples without solvent exchange, and with solvent exchange in water or ammonia at different concentrations (0.01N, 0.1N, 1N, and 3N) are shown in Figure 2A. Here and in subsequent presentation of porosimetry data, V is the cumulative pore volume, and D is the pore diameter. Therefore, the plot of dV/dLog(D) versus D represents the pore size distribution. It is readily seen from the figure that the solvent exchange process enlarges the pore size, decreases the surface area, and slightly increases the pore volume. As the concentration of ammonia increases, the effect intensifies. This trend is in agreement with results published for sol-gel-derived silica.[48,49]

TEM images of the samples without solvent exchange and of those immersed in 0.01N and 3N ammonia for solvent exchange are shown in Figure 2B. For the sample without solvent exchange (Fig. 2B, panel a), the mass contrast can barely be resolved, indicating that the sample is homogeneous to the level of the resolution limit for the given sample thickness (~100 nm). When the samples are soaked in ammonia, some dark, irregular shaped domains develop inside the gel matrix with lighter channels located

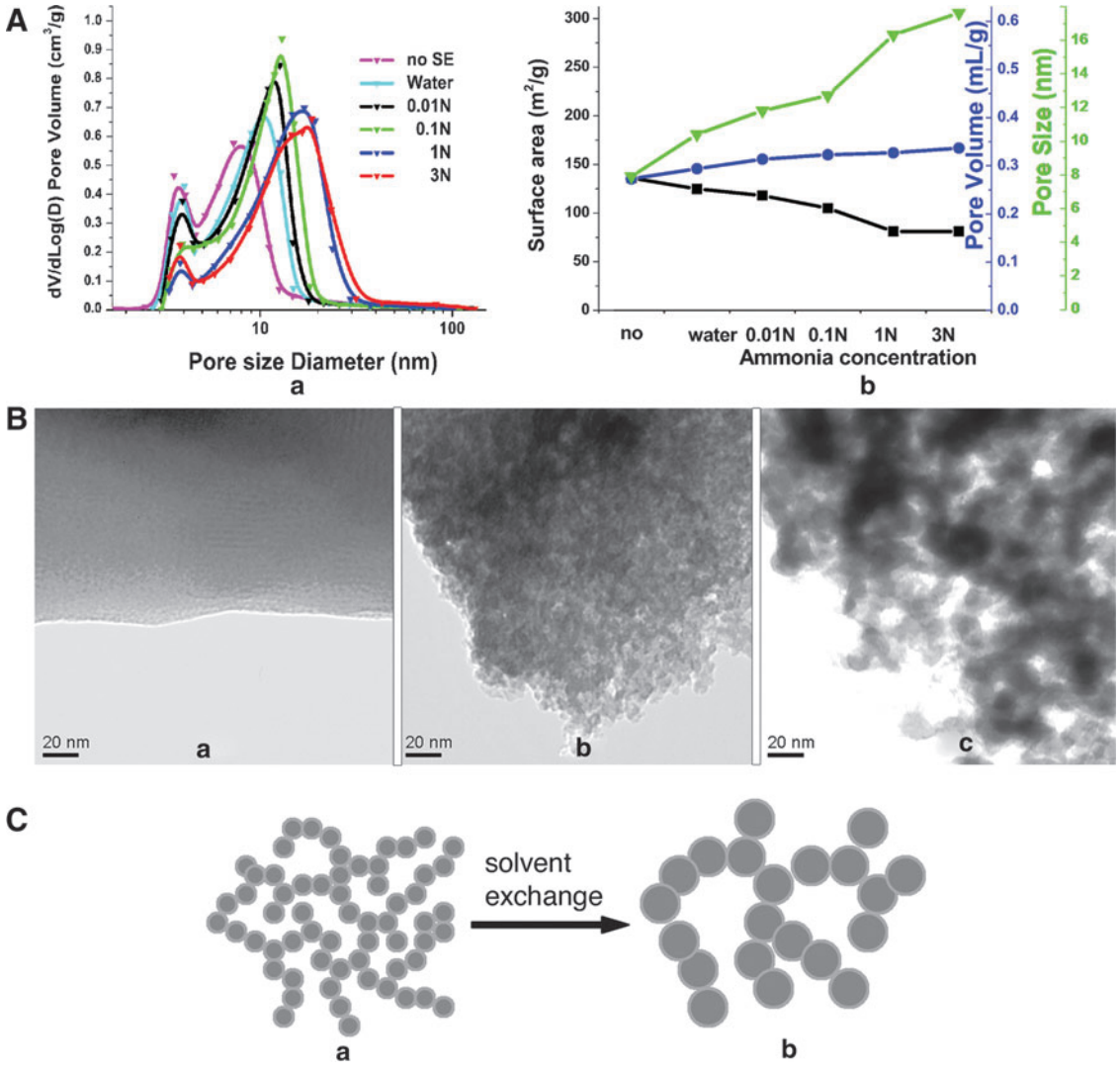

FIG. 2. **(A)** Effect of solvent exchange on pore size distribution **(**in **a)**, and surface area (black squares), nanopore volume (blue circles), and median nanopore size (green triangles) **(**in **b)** of BG scaffolds. The samples without solvent exchange are shown for reference against the ones immersed in water or ammonia at different concentrations (0.01N, 0.1N, 1N, and 3N) for solvent exchange. **(B)** TEM micrographs of samples without solvent exchange (a), and with solvent exchange in 0.01N **(b)**, or 3N ammonia **(c)**. Note the increasing porosity in samples **(a)** to **(c)**. **(C)** Schematic representation depicting the nanostructure evolution in gel networks during the solvent exchange process: gel network before **(a)** and after **(b)** the solvent exchange process. Color images available online at www.liebertpub.com/tea

in between them (Fig. 2B, panels b and c). The size of domains and channels increases with the increasing ammonia concentration.

Based on our TEM and nitrogen adsorption analyses, the mechanism of solvent exchange can be explained by the dissolution of silica in wet gel before stabilization. The dissolution rate of silica in basic solution is significantly higher than that in an acidic solution.[50,51] In the basic solution, the highly soluble smaller clusters dissolve and re-precipitate on the larger clusters, representing an example of classic Ostwald ripening. As a result, the gel network becomes coarser, leading to larger clusters (appearing as dark, irregular shaped domains in TEM micrographs as shown in Fig. 2B, panels b and c) and greater inter-cluster spacing (namely, the lighter channels between dark irregular-shaped domains). The inter-cluster spaces are nanopores detected by the nitrogen adsorption technique. A schematic of nanostructure evolution during the solvent exchange process is shown in Figure 2C.

The role of nanoporosity on the performance of BG scaffolds

It is well known that surface topography can have a significant impact on cell behavior.[52,53] For example, rougher Ti surfaces promote bone formation while smoother surfaces tend to stimulate the formation of a fibrous interface.[54,55] In contrast, for BG, cells have been reported to attach and proliferate better on smoother surfaces.[56,57] However, the topology scales in these studies are at the micron level size that is comparable to the size of cells. They are orders of magnitude larger than the nanopore scale investigated in the present study.

To establish the role of nanoporosity on the *in vivo* tissue response, two batches of BG samples with significantly different nanoporosity were fabricated and implanted subcutaneously into New Zealand rabbits. Sample A represented a typical nano–macro dual porous BG scaffold sintered at 700°C, whereas sample B was sintered at 840°C. The higher sintering temperature eliminated most of the nanoporosity as confirmed by the nanopore size distribution analysis of the two samples (Fig. 3A).

In vivo animal tissue response to scaffolds A and B was examined 1 and 2 weeks postimplantation (Fig. 3B). After 1 week postimplantation, cells penetrated more than 200 μm deep into the macropores of sample A (the BG scaffold with nano–macro dual pores, Fig. 3B, panel a). By comparison, there was no clear sign of cell penetration in sample B after 1 week (the BG scaffold with negligible nanoporosity, Fig. 3B, panel b). By 2 weeks postimplantation, cells also began to penetrate the macropores of sample B (Fig. 3B, panel d); however, the depth of penetration ($\sim$400 μm) and the amount of cells colonizing the inside of the macropores remained significantly below that observed for sample A (Fig. 3B, panel c). These observations strongly support the beneficial effect of nanopores incorporated into BG scaffolds.

The beneficial effect of nanopores on tissue regeneration is further confirmed by comparing the level of tissue integration to nanoporous (sample C, nanopores but no macropores) versus "bulk" BG scaffolds (no nano- or macropores, sample D). Two weeks postimplantation, tissue fully integrated with the nanoporous BG scaffold (sample C in Fig. 4, left panel). However, clearly visible interstitial spaces (marked by red arrows in sample D, Fig. 4, right panel) remained between bulk BG scaffolds and surrounding tissue, indicating a relatively poor scaffold integration.

It is well known that cell attachment, migration, and growth can be mediated by proteins that absorb from serum on the surface of biomaterials.[29] Furthermore, for BG, the appropriate concentration of silicate and calcium ions released from the surface can stimulate the formation and growth of bone nodules.[3] The incorporation of nanopores enhances the surface area, which, in principle, can provide an increased number of sites for protein adsorption, as well as ion concentrations optimized for more efficient cell growth.

The role of nanopore topology on cell response

Although the benefit of nanopores in BG scaffolds has been demonstrated by our observations presented in Figures 3 and 4, the question remains whether the beneficial effects are related purely to the increase of surface area that occurs concurrently with the modification of nanopores, or whether they are also related to the topography of nanopores. Note that the optimal concentration of ionic products of dissolution, especially the silicate and Ca^{2+} ions released from a BG surface, is important for bone regeneration.[3] On the other hand, proteins can bond to the BG surface,[58] and thus mediate cell attachment, migration, and growth.[29] These surface area-regulated protein absorption and ion release processes can greatly affect the performance of a biomaterial.

To be able to exclude any effects of surface area, and to prove a beneficial effect of nanopore topology, cell response should be compared between samples that have comparable surface area but significantly different pore size. We succeeded in preparing two sample batches (E and F) meeting these requirements. Samples E were soaked in 3N ammonia for solvent exchange and sintered at 700°C, while samples F were sintered at 750°C and were not subjected to any solvent exchange. Note that the 70%SiO_2–30%CaO composition forms highly stable glass by the sol-gel method, which is not affected chemically by these sintering treatments. Surface area and pore size measured by nitrogen adsorption revealed that the two scaffolds had almost identical surface areas (83 ± 2 and $81 \pm 2\ m^2/g$, respectively), but significantly different average pore sizes (17.7 nm for samples E and 3.7 nm for samples F) (Fig. 5A).

To specifically examine the influence of nanopore topology on cell behavior, *in vitro* response of MC3T3-E1 mouse preosteoblast cells to these two types of BG scaffolds was evaluated 12 and 48 h post cell seeding using triplicate samples ($n = 3$) (Fig. 5B). Within 12 h post seeding, cells attached to the surface of both sample types, and began to proliferate within 24 h. As indicated by cellular actin-cytoskeleton staining (green), cells on all specimens exhibited a well-spread epitheloid-like morphology featuring prominent stress fibers as is typical for cells adhering to stiff substrates (Fig. 5B); however, cell density on sample F was significantly higher than on sample E 12 h post seeding (Fig. 5C). The difference in cell density on the two sample types (quantified by manually counting DAPI-stained cell nuclei, blue) was less pronounced by 48 h post seeding, although a slightly higher density of cells was detected on samples F (with smaller nanopore size) than on samples E (Fig. 5C). No obvious differences in actin organization were observed

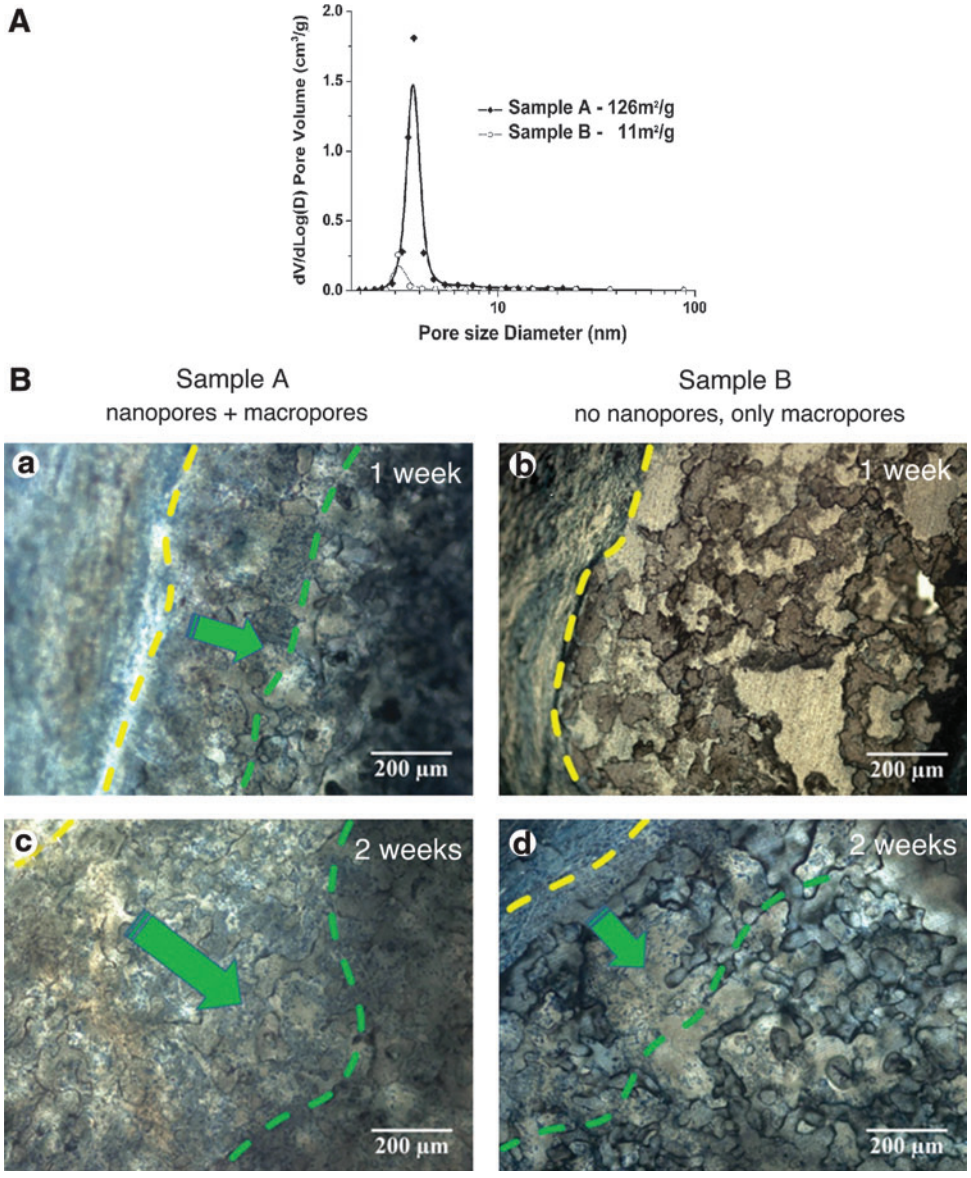

FIG. 3. **(A)** Nanopore size-distribution as determined by BET measurements of nitrogen absorption. Samples A (solid diamond) were sintered at 700°C and samples B (open circle) were sintered at 840°C. **(B)** Micrographs showing representative histological results of samples subcutaneously implanted into rabbits. **(a)** Samples A (nano–macro dual porous BG scaffolds) 1 week postimplantation; **(b)** Samples B (scaffolds with macropores only) 1 week postimplantation; **(c)** Samples A 2 weeks postimplantation; **(d)** Samples B 2 weeks postimplantation. The yellow lines delineate the tissue and BG scaffold interfaces. The green lines delineate the depth of cell penetration (from left to right, demarked by green arrows) into the BG scaffolds. Sections were stained with Stevenel's blue and Van Gieson to reveal connective tissue (bluish green) and hard tissue (red), respectively. Color images available online at www.liebertpub.com/tea

between the two scaffold types on these relatively low magnified samples. Taken together, these results indicate that smaller nanopore size promotes scaffold cell adhesion but does not significantly affect subsequent cell proliferation.

Discussion

Recently, the impact of nanostructure on cell functions has been studied on various material systems.[28–34,36] In these studies, cell performance was enhanced by introducing nanostructures, such as nanocarbon/-polymer fibers, or nanopores to the scaffolds. Results obtained in these studies correlate well with our *in vitro* and *in vivo* observations (Figs. 3–5). However, how precisely nanostructure influences cell performance is still unclear and under debate. For example, Woo *et al.* suggested that incorporation of nanostructures would lead to an increased surface area, promoting protein adsorption, and hence improved cell attachment.[29] Others have suggested that nanopore topography directly influences cellular

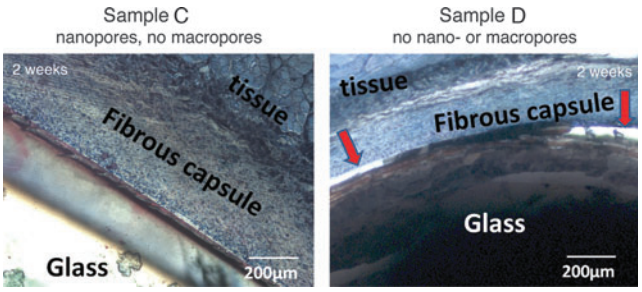

FIG. 4. Micrographs showing representative histological results of nanoporous BG scaffolds (samples C, left panel) and nonporous BG scaffolds (samples D, right panel) 2 weeks postimplantation. Red arrows mark the interstitial space that remained between the nonporous sample and tissue in (right panel), while tissue fully integrated with the nanoporous BG scaffold (left panel). Color images available online at www.liebertpub.com/tea

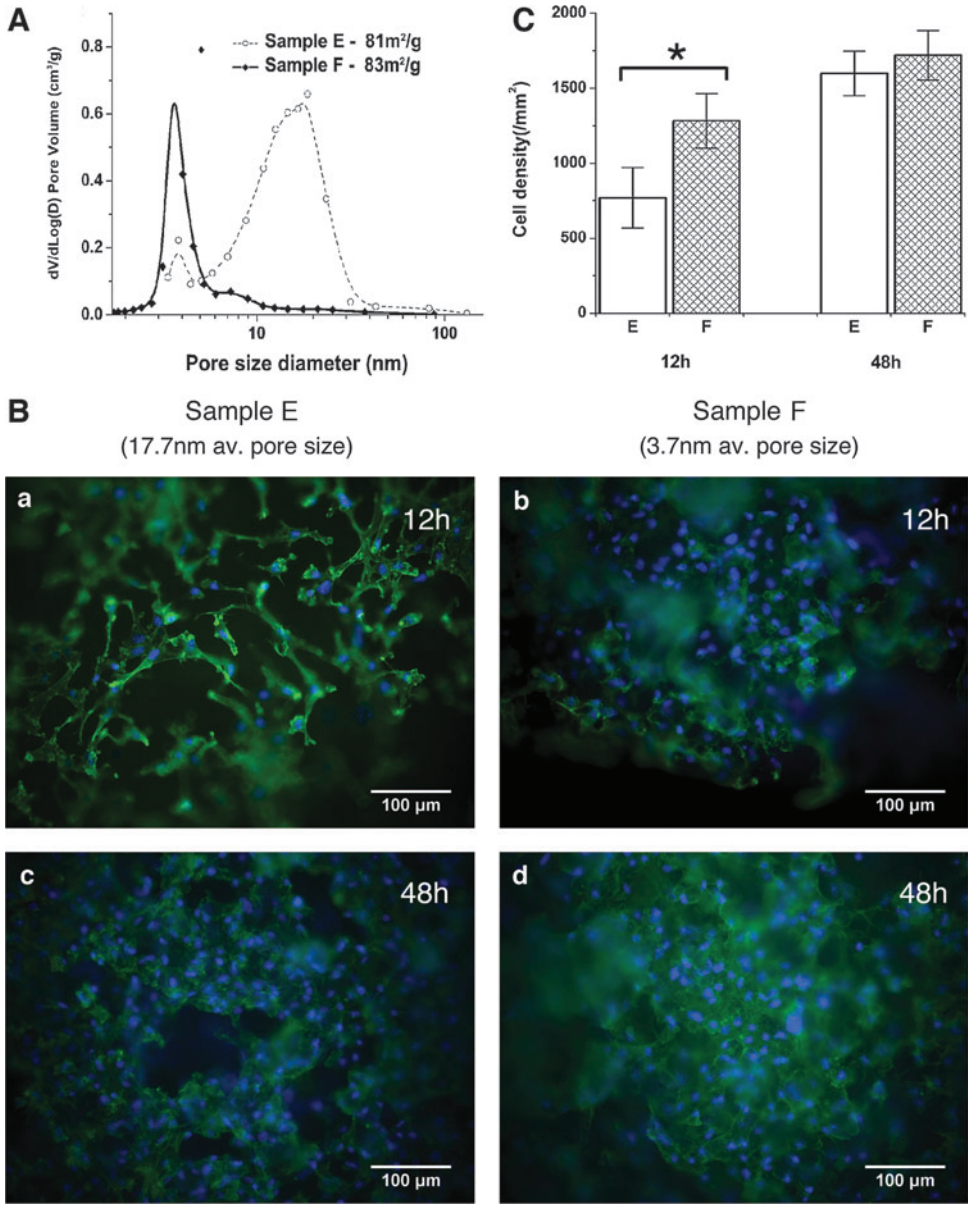

FIG. 5. **(A)** Pore size distribution of samples E and F. **(B)** Representative micrographs of **(a)** samples E at 12 h, **(b)** samples F at 12 h, **(c)** samples E at 48 h, and **(d)** samples F at 48 h post cell seeding. MC3T3-E1 mouse calvarial bone preosteoblast cells were fixed with formaldehyde, F-actin was stained with Alexa 488-Phalloidin (green) to evaluate cell morphology, and cell nuclei were stained with DAPI (blue) to quantify cell density. Images were acquired using a 20× objective. **(C)** Cell density on samples E and F 12 and 48 h after cell seeding. The error bars represent the standard deviation of cell density on three samples (*statistically significant, $p < 0.05$). Color images available online at www.liebertpub.com/tea

functions, either by enhancing protein adsorption,[33] changing the conformation of certain cellular attachment proteins,[59] or by changing the surface energy.[32,36] Unfortunately, in these studies a change of nanostructure size was always coupled with a concurrent variation of surface area. Therefore, it remained ambiguous whether observed beneficial effects were due to the increase in surface area, or were also influenced by the topography of nanostructure. A recent *in vitro* study investigated the influence of surface characteristics of polymethyl-methacrylate on bone formation.[60] The results suggest that a distinct arrangement of nanoscale disorder can stimulate mesenchymal stem cells to produce bone mineral *in vitro*, even under conditions where all other parameters (e.g., the size and number of nanopits) remained unchanged, supporting our findings that nanotopography plays an important role for cellular performance.

Our results presented here indicate that nanotopography of bioscaffolds affects the early phases of cell adhesion, and potentially modulates other characteristics, such as cell morphology and gene expression. Clearly, many more samples with a range of nanopore size (but with the same surface area) would need to be examined to establish the optimum pore size for the adhesion of a specific cell type. Although the underlying mechanisms that lead to differences in cell attachment was not fully explored in our study, a previous study conducted on alumina suggests that the unfolding of the cellular adhesion protein, vitronectin, by introducing nanophase, could expose an increased number of cell-adhesive epitopes that then are recognized by specific cell-membrane receptors, leading to enhanced cell attachment.[59] Based on these findings it is tempting to speculate that conformational changes of specific cellular adhesion proteins in response to different nanotopology may be responsible for the observed cell attachment differences in our study. Furthermore, one likely explanation for the decreasing impact of nanopore size at later time points (48 h) is that with time the scaffold surface developed a coating of cell-secreted proteins, which obscured the influence of underlying nanoscale topology.

Concluding Remarks

We have demonstrated that the nanostructure, specifically the nanoporosity, of the TAMP scaffolds can be tailored by manipulating the sintering temperature and/or ammonia concentration used during the solvent exchange process. Although both techniques lower the overall surface area of BG scaffolds, the former process closes nanopores through densification, whereas the latter one enlarges nanopore size through the coarsening of the gel network. Thus, TAMP scaffolds with different pore sizes but comparable surface area can be generated by combining these two methods.

Furthermore, the study of *in vivo* animal tissue response indicates that nanoporosity promotes cell penetration into TAMP scaffolds, underscoring the beneficial effect of incorporation of nanopores. Finally, *in vitro* cell tests on BG scaffolds with similar surface area but different nanopore size indicate that initial cell attachment is significantly enhanced on BG scaffolds with smaller pore size. In conclusion, this study provides the first unambiguous evidence that nanoscale topology alone can significantly affect the biological performance of engineered glass tissue scaffolds.

Acknowledgments

S.W. would like to thank Ahmad Rashad for assistance with *in vivo* animal experiments. We thank the National Science Foundation for supporting this work via Materials World Network (DMR-0602975) and International Materials Institute for New Functionality in Glass (IMI-NFG, DMR-0844014) programs. The work in the laboratory of MMF is supported by the National Institutes of Health (NIH-NIGMS, Grant R01 GM55725).

Disclosure Statement

No competing financial interests exist.

References

1. Griffon, D.J. Evaluation of osteoproductive biomaterials: allograft, bone inducing agent, bioactive glass, and ceramics. Department of Clinical Veterinary Sciences, Division of Surgery, University of Helsinki, Helsinki, 2002.
2. Pereira, M.M., Jones, J.R., and Hench, L.L. Bioactive glass and hybrid scaffolds prepared by sol–gel method for bone tissue engineering. Adv Appl Ceramics **104,** 35, 2005.
3. Hench, L.L. The story of Bioglass. J Mater Sci-Mater Med **17**, 967, 2006.
4. Hutmacher, D.W. Scaffolds in tissue engineering bone and cartilage. Biomaterials **21,** 2529, 2000.
5. Rezwan, K., Chen, Q.Z., Blaker, J.J., and Boccaccini, A.R. Biodegradable and bioactive porous polymer/inorganic composite scaffolds for bone tissue engineering. Biomaterials **27,** 3413, 2006.
6. Freyman, T.M., Yannas, I.V., and Gibson, L.J. Cellular materials as porous scaffolds for tissue engineering. Prog Mater Sci **46,** 273, 2001.
7. Griffith, L.G. Emerging design principles in Biomaterials and scaffolds for tissue engineering. In: Sipe, J.D., Kelley, C.A., and McNicol, L.A., eds. Reparative Medicine: Growing Tissues and Organs, New York: New York Academy of Sciences, 2002, pp. 83–95.
8. Jones, J.R., Lee, P.D., and Hench, L.L. Hierarchical porous materials for tissue engineering. Philos Trans R Soc A-Math Phys Eng Sci **364,** 263, 2006.
9. Karageorgiou, V., and Kaplan, D. Porosity of 3D biornaterial scaffolds and osteogenesis. Biomaterials **26,** 5474, 2005.
10. Ramay, H.R., and Zhang, M.Q. Preparation of porous hydroxyapatite scaffolds by combination of the gel-casting and polymer sponge methods. Biomaterials **24,** 3293, 2003.
11. Chen, Q.Z.Z., Thompson, I.D., and Boccaccini, A.R. 45S5 Bioglass (R)-derived glass-ceramic scaffolds for bone tissue engineering. Biomaterials **27,** 2414, 2006.
12. Fu, Q., Rahaman, M.N., Bal, B.S., Brown, R.F., and Day, D.E. Mechanical and *in vitro* performance of 13–93 bioactive glass scaffolds prepared by a polymer foam replication technique. Acta Biomater **4,** 1854, 2008.
13. Vitale-Brovarone, C., Baino, F., and Verne, E. High strength bioactive glass-ceramic scaffolds for bone regeneration. J Mater Sci-Mater Med **20,** 643, 2009.
14. Michna, S., Wu, W., and Lewis, J.A. Concentrated hydroxyapatite inks for direct-write assembly of 3-D periodic scaffolds. Biomaterials **26,** 5632, 2005.
15. Kaufmann, E., Ducheyne, P., and Shapiro, I.M. Evaluation of osteoblast response to porous bioactive glass (45S5) substrates by RT-PCR analysis. Tissue Eng **6,** 19, 2000.
16. Livingston, T., Ducheyne, P., and Garino, J. *In vivo* evaluation of a bioactive scaffold for bone tissue engineering. J Biomed Mater Res **62,** 1, 2002.
17. Liang, W., Rahaman, M.N., Day, D.E., Marion, N.W., Riley, G.C., and Mao, J.J. Bioactive borate glass scaffold for bone tissue engineering. J Non-Cryst Solids **354,** 1690, 2008.
18. Fu, Q., Rahaman, M.N., Bal, B.S., and Brown, R.F. Preparation and *in vitro* evaluation of bioactive glass (13–93) scaffolds with oriented microstructures for repair and regeneration of load-bearing bones. J Biomed Mater Res Part A **93A,** 1380, 2010.
19. Brown, R.F., Day, D.E., Day, T.E., Jung, S., Rahaman, M.N., and Fu, Q. Growth and differentiation of osteoblastic cells on 13–93 bioactive glass fibers and scaffolds. Acta Biomater **4,** 387, 2008.
20. Zhang, D., Jain, H., Hupa, M., and Hupa, L. *In-vitro* Degradation and Bioactivity of Tailored Amorphous Multi Porous Scaffold Structure. J Am Ceram Soc **95,** 2687, 2012.
21. Moawad, H.M.M., and Jain, H. Creation of nano-macro-interconnected porosity in a bioactive glass-ceramic by the melt-quench-heat-etch method. J Am Ceram Soc **90,** 1934, 2007.
22. Sepulveda, P., Jones, J.R., and Hench, L.L. Bioactive sol-gel foams for tissue repair. J Biomed Mater Res **59,** 340, 2002.
23. Lofton, C.M., Milz, C.B., Huang, H.Y., and Sigmund, W.M. Bicontinuous porosity in ceramics utilizing polymer spinodal phase separation. J European Ceram Soc **25,** 883, 2005.
24. Marques, A.C., Jain, H., and Almeida, R.M. Sol-gel derived nano/macroporous scaffolds. Phys Chem Glasses-Eur J Glass Sci Technol Part B **48,** 65, 2007.
25. Wang, S.J., and Jain, H. High surface area nanomacroporous bioactive glass scaffold for hard tissue engineering. J Am Ceram Soc **93,** 3002, 2010.
26. Goldberg, M., Langer, R., and Jia, X.Q. Nanostructured materials for applications in drug delivery and tissue engineering. J Biomater Sci-Polym Ed **18,** 241, 2007.
27. Grausova, L., Kromka, A., Burdikova, Z., Eckhardt, A., Rezek, B., Vacik, J., Haenen, K., Lisa, V., and Bacakova, L. Enhanced growth and osteogenic differentiation of human osteoblast-like cells on boron-doped nanocrystalline diamond thin films. PLoS One **6,** 1, 2011.

28. Elias, K.L., Price, R.L., and Webster, T.J. Enhanced functions of osteoblasts on nanometer diameter carbon fibers. Biomaterials **23,** 3279, 2002.
29. Woo, K.M., Chen, V.J., and Ma, P.X. Nano-fibrous scaffolding architecture selectively enhances protein adsorption contributing to cell attachment. J Biomed Mater Res Part A **67A,** 531, 2003.
30. Huang, J., Best, S.M., Bonfield, W., Brooks, R.A., Rushton, N., Jayasinghe, S.N., and Edirisinghe, M.J. *In vitro* assessment of the biological response to nano-sized hydroxyapatite. J Mater Sci-Mater Med **15,** 441, 2004.
31. Teixeira, A.I., Nealey, P.F., and Murphy, C.J. Responses of human keratocytes to micro- and nanostructured substrates. J Biomed Mater Res Part A **71A,** 369, 2004.
32. Dalby, M.J., Biggs, M.J.P., Gadegaard, N., Kalna, G., Wilkinson, C.D.W., and Curtis, A.S.G. Nanotopographical stimulation of mechanotransduction and changes in interphase centromere positioning. J Cell Biochem **100,** 326, 2007.
33. Misra, S.K., Mohn, D., Brunner, T.J., Stark, W.J., Philip, S.E., Roy, I., Salih, V., Knowles, J.C., and Boccaccini, A.R. Comparison of nanoscale and microscale bioactive glass on the properties of P(3HB)/Bioglass (R) composites. Biomaterials **29,** 1750, 2008.
34. Marques, A.C., Almeida, R.M., Thiema, A., Wang, S.J., Falk, M.M., and Jain, H. Sol-gel-derived glass scaffold with high pore interconnectivity and enhanced bioactivity. J Mater Res **24,** 3495, 2009.
35. Zhang, L.J., and Webster, T.J. Nanotechnology and nanomaterials: promises for improved tissue regeneration. Nano Today **4,** 66, 2009.
36. Raimondo, T., Puckett, S., and Webster, T.J. Greater osteoblast and endothelial cell adhesion on nanostructured polyethylene and titanium. Int J Nanomed **5,** 647, 2010.
37. Ahmad, M., Jones, J.R., and Hench, L.L. Fabricating sol-gel glass monoliths with controlled nanoporosity. Biomed Mater **2,** 6, 2007.
38. Lin, S., Ionescu, C., Valliant, E.M., Hanna, J.V., Smith, M.E., and Jones, J.R. Tailoring the nanoporosity of sol-gel derived bioactive glass using trimethylethoxysilane. J Mater Chem **20,** 1489, 2010.
39. Jones, J.R., Ehrenfried, L.M., and Hench, L.L. Optimising bioactive glass scaffolds for bone tissue engineering. Biomaterials **27,** 964, 2006.
40. Takahashi, R., Nakanishi, K., and Soga, N. Effects of aging and solvent exchange on pore structure of silica-gels with interconnected macropores. J Non-Cryst Solids **189,** 66, 1995.
41. Wang, S.J., Falk, M.M., Rashad, A., Saad, M.M., Marques, A.C., Almeida, R.M., Marei, M.K., and Jain, H. Evaluation of 3D nano-macro porous bioactive glass scaffold for hard tissue engineering. J Mater Sci Mater Med **22,** 1195, 2011.
42. Brunauer, S., Emmett, P.H., and Teller, E. Adsorption of gases in multimolecular layers. J Am Chem Soc **60,** 309, 1938.
43. Barrett, E.P., Joyner, L.G., and Halenda, P.P. The determination of pore volume and area distributions in porous substances .1. computations from nitrogen isotherms. J Am Chem Soc **73,** 373, 1951.
44. Council, N.R. Guide for the Care and Use of Laboratory Animals, 2nd Ed. Washington, D.C.: National Academy Press, Institute of Laboratory Animal Resources, 1996, pp. 56–76.
45. Marei, M.K., Nouh, S.R., Saad, M.M., and Ismail, N.S. Preservation and regeneration of alveolar bone by tissue-engineered implants. Tissue Eng **11,** 751, 2005.
46. James, K.S., Zimmerman, M.C., and Kohn, J. Small animal surgical and histological procedures for characterizing the performance of tissue-engineered bone grafts. In: Jeffrey R. Morgan and Martin L. Yarmush, eds., Tissue Engineering Methods and Protocols. Totowa, NJ: Humana Press, 1999, pp. 121–131.
47. Barsoum, M. Fundamentals of Ceramics, Chapter 10. New York: Taylor & Francis, 2003.
48. Nakanishi, K., Takahashi, R., Nagakane, T., Kitayama, K., Koheiya, N., Shikata, H., and Soga, N. Formation of hierarchical pore structure in silica gel. J Sol-Gel Sci Technol **17,** 191, 2000.
49. Nakanishi, K. Pore structure control of silica gels based on phase separation. J Porous Mater **4,** 67, 1997.
50. Brinker, C.J., and Scherer, G.W. Sol-Gel Science: The Physics and Chemistry of Sol-Gel Processing. San Diego, CA: Academic Press, 1990.
51. Brinker, C.J. Hydrolysis and condensation of silicates - effects on structure. J Non-Cryst Solids **100,** 31, 1988.
52. Boyan, B.D., Hummert, T.W., Dean, D.D., and Schwartz, Z. Role of material surfaces in regulating bone and cartilage cell response. Biomaterials **17,** 137, 1996.
53. Engel, E., Martinez, E., Mills, C.A., Funes, M., Planell, J.A., and Samitier, J. Mesenchymal stem cell differentiation on microstructured poly (methyl methacrylate) substrates. Ann Anat-Anat Anz **191,** 136, 2009.
54. Schwartz, Z., and Boyan, B.D. Underlying mechanisms at the bone-biomaterial interface. J Cell Biochem **56,** 340, 1994.
55. Mwenifumbo, S., Li, M.W., Chen, J.B., Beye, A., and Soboyejo, W. Cell/surface interactions on laser micro-textured titanium-coated silicon surfaces. J Mater Sci-Mater Med **18,** 9, 2007.
56. Jain, R.H., Wang, S.J., Moawad, H.M.M., Falk, H.M., and Jain, H. Glass bone implants: the effect of surface topology on attachment and proliferation of osteoblast cells on 45S bioactive glass. Mater Res Soc Symp Proc **1235,** 2010.
57. Levy, S., Van Dalen, M., Agonafer, S., and Soboyejo, W.O. Cell/surface interactions and adhesion on bioactive glass 45S5. J Mater Sci-Mater Med **18,** 89, 2007.
58. Lenza, R.F.S., Jones, J.R., Vasconcelos, W.L., and Hench, L.L. *In vitro* release kinetics of proteins from bioactive foams. J Biomed Mater Res Part A **67A,** 121, 2003.
59. Webster, T.J., Schadler, L.S., Siegel, R.W., and Bizios, R. Mechanisms of enhanced osteoblast adhesion on nanophase alumina involve vitronectin. Tissue Eng **7,** 291, 2001.
60. Dalby, M.J., Gadegaard, N., Tare, R., Andar, A., Riehle, M.O., Herzyk, P., Wilkinson, C.D.W., and Oreffo, R.O.C. The control of human mesenchymal cell differentiation using nanoscale symmetry and disorder. Nat Mater **6,** 997, 2007.

Address correspondence to:
Himanshu Jain, EngScD
Department of Materials Science and Engineering
Lehigh University
Bethlehem, PA 18015

E-mail: h.jain@lehigh.edu

Matthias M. Falk, PhD
Department of Biological Sciences
Lehigh University
Bethlehem, PA 18015

E-mail: mfalk@lehigh.edu

Received: September 27, 2012
Accepted: February 18, 2013
Online Publication Date: March 25, 2013